Available online at www.sciencedirect.com
ScienceDirect
Journal of Sound and Vibration 322 (2009) 454–474
JOURNAL OF SOUND AND VIBRATION
www.elsevier.com/locate/jsvi

Measurement and modelling of the *y*-direction apparent mass of sitting human body–cushioned seat system

George Juraj Stein[a,*], Peter Múčka[a], Barbara Hinz[b], Ralph Blüthner[b]

[a]*Institute of Materials and Machine Mechanics, Slovak Academy of Sciences, Račianska 75, SK–831 02 Bratislava 3, Slovak Republic*
[b]*Federal Institute for Occupational Safety and Health, Vibration and Electromagnetic Fields, Nöldnerstrasse 40-42, D-10317 Berlin, Germany*

Received 4 December 2007; received in revised form 30 July 2008; accepted 5 November 2008
Handling Editor: C.L. Morfey
Available online 3 January 2009

Abstract

Laboratory tests were conducted using 13 male subjects seated on a cushioned commercial vehicle driver's seat. The hands gripped a mock-up steering wheel and the subjects were in contact with the lumbar region of the backrest. The accelerations and forces in the *y*-direction were measured during random lateral whole-body vibration with a frequency range between 0.25 and 30 Hz, vibration magnitudes 0.30, 0.98, and 1.92 $m\,s^{-2}$ (unweighted root mean square (rms)).

Based on these laboratory measurements, a linear multi-degree-of-freedom (mdof) model of the seated human body and cushioned seat in the lateral direction (*y*-axis) was developed. Model parameters were identified from averaged measured apparent mass values (modulus and phase) for the three excitation magnitudes mentioned. A preferred model structure was selected from four 3-dof models analysed. The mean subject parameters were identified. In addition, identification of each subject's apparent mass model parameters was performed. The results are compared with previous studies. The developed model structure and the identified parameters can be used for further biodynamical research in seating dynamics.

1. Introduction

The biodynamic response of human body to vibration and shock is a complex problem that has been the subject of permanent research. The most comprehensive description of all the aspects can be found, e.g., in [1,2] and in abridged way in [3]. It continues to be challenging to develop a sufficiently accurate but reasonable simple model for the human body in various practical positions, e.g., sitting in a suspended cushioned driver's seat in working environment or in an unsuspended and partially reclined cushioned passenger car seat. Much work on the measurement and modelling of human body response has been done for the vertical (*z*-axis) direction, e.g., [2–7], to name but a few. Mathematical models of the vertical apparent mass of an upright sitting human body on a rigid seat have been developed for example in [7–11] and are described in condensed form in [12].

*Corresponding author. Tel.: +4212 5930 9422; fax: +4212 5477 2909.
E-mail address: stein@savba.sk (G.J. Stein).

0022-460X/$ - see front matter
doi:10.1016/j.jsv.2008.11.002

1.1. Published apparent mass measurement data for the x- and y-directions

The most comprehensive human body response measurements in the fore-and-aft direction (x-axis) and in the lateral direction (y-axis) have been reported in [4,13,14] and recently in [15–22].

Papers [4,13,14] were concerned with the measurement of human body sitting upright on a rigid seat in a well-defined biodynamical position without interaction with controls or the seat back. Few papers have been concerned with the influence of the seat-back support [4,15,17,20,21]. Authors have generally assumed a rigid, vertical seat-back support without any cushioning. Some of these measurements were performed with single axis excitation, other with dual or triple axis excitation [19,22]. In paper [17] the general influence of the back-contact was examined using three different cases, no back contact, back contact with upright standing rigid back support and a backwards reclined rigid back-support in the so-called automobile posture position. Other papers dealing with analysis of passenger car seats have also been published [23–26]. However, the driver and passenger's posture is different from the posture typically observed in industrial environment and the reported excitation intensities are lower than in the latter case. Despite some similarities, automotive and industrial seats classes require different test conditions.

1.2. Models of apparent mass in the horizontal directions

In the fore-and-aft and lateral directions, little work on apparent mass modelling has been hitherto reported with the exception being probably the work by Mansfield and Lundström [27]. This model is relevant to a test subject sitting upright on a rigid seat without any seat-back support. It was based on then available data, specifically on those of [4,14]. Various three-degree-of-freedom (3-dof) models were presented with parameters determined from the apparent mass modulus only. The Nelder and Mead algorithm was used. As seen from respective figures in [27], the match between the measured and simulated apparent mass phase differs markedly for frequencies larger than 4 Hz. Below this frequency the differences are smaller. Hence, the models can be assumed to reasonably represent the real situation only up to this frequency.

Recently, Fleury and Mistrot [28] described a fore-and-aft (x-direction) human body model using rotary and translatory mechano-mathematical elements. They used this model to predict the x-direction vibration attenuation from a driver's seat equipped with a fore-and-aft suspension system. Stein et al. [29] described another x-direction model of the human body sitting in an upright position with a suspended and cushioned seat upper part using linear translatory mechano-mathematical elements. This model was used for assessing the influence of the back contact of the seated driver and the influence of introducing a steering wheel. This x-direction apparent mass model was further used to identify model parameters based on measurements with a group of test persons described in detail in [30].

There are currently no reliable models of the human body-cushioned seat upper part system in the y-direction. This paper presents a reasonable simple mechano-mathematical model that is justified from physical and biodynamical point of view.

2. Determination of the apparent mass in the y-direction

2.1. Definition of the apparent mass function

The biodynamic response of the seated human body has often been evaluated in terms of the driving point impedance or apparent mass in relation to the force and the acceleration at the interface between subject and the seat, e.g., [2,3,31]. This method indicates the presence of resonances in the human body–seat system [3]. The apparent mass is a well-established descriptor in biodynamics and in human influence of vibrations research as described by [2,3,5,31]. ISO 5982 [31] defines the apparent mass $\mathbf{M}_a$ for the vertical direction (z-axis) as the complex ratio of the spectrum of the resulting force $\mathbf{F}$ and the spectrum of the excitation acceleration $\mathbf{a}$, measured at the same point and in the same direction:

$$\mathbf{M}_a(f) = \frac{\mathbf{F}(f)}{\mathbf{a}(f)}. \tag{1}$$

More generally, the apparent mass $\mathbf{M}_a(\omega)$ as a function of positive angular frequency $\omega = 2\pi f$ within a given frequency range is the complex ratio of the force $\mathbf{F}(\omega)$ applied to the system and the resulting motion (acceleration $\mathbf{a}(\omega)$) at the same point and the same direction, both being complex quantities:

$$\mathbf{M}_a(\omega) = \frac{\mathbf{F}(\omega)}{\mathbf{a}(\omega)}. \tag{2}$$

However, it is much more practical to generate required acceleration excitation (harmonic or random) and measure the resultant force, see for example [22,25]. Hence, the apparent mass is estimated in practice using this approach.

2.2. Experimental data

In the case reported here, 13 male subjects with body masses between 62.2 and 103.6 kg and body heights between 174 and 196 cm were used for the tests. The individual anthropometrical parameters and the body mass index (BMI) are given in Table 1. The subjects were exposed to random whole-body vibration in y-direction (nearly flat spectrum from 0.25 to 30 Hz for 65 s) with unweighted rms values: $e1 = 0.30\,\mathrm{m\,s^{-2}}$, $e2 = 0.98\,\mathrm{m\,s^{-2}}$, and $e3 = 1.92\,\mathrm{m\,s^{-2}}$. These exposures were generated by the control system of a hexapod simulator modified for human experiments. The requirements of ISO 13090-1 [32] were taken into consideration. The twofold exposition to different vibration magnitudes was balanced across the subjects.

Test subjects sat in a relaxed upright posture on upper part of a heavy commercial vehicle driver's seat with an integrated backrest and with the hands gripping a device simulating the steering wheel. The vertical suspension system was not present (Fig. 1). For safety reasons a seat belt was used (cf. Fig. 1). However, as observed during all exposures, the seat belt was loose and did not interfere with the movement of the tested person. The curved lower part of the backrest cushion had an inclination between 17° and 28°. The subjects were instructed to maintain contact with the backrest in the lumbar region only and to maintain this posture during the test (cf. Fig. 1). The measurement set-up was identical to that one described in more detail in [22], except that a cushioned seat upper part was used.

The upper part of the cushioned seat was mounted on a Kistler force plate Type 9366AB, which was integrated into a rigid structure supporting the seat. The feet of the test subjects were supported by a plate on the simulator, which moved in the same way as the force plate. The forces were measured by the Kistler force plate and were amplified using a matched eight-channel amplifier (Kistler 9865B). Accelerations were measured at the Kistler force plate by three capacitance accelerometers type ENDEVCO 7290A-10 mounted

Table 1
Body masses, body heights, and BMI (Body Mass Index) of the 13 male subjects.

Subject number	Body mass (kg)	Body height (cm)	BMI ($\mathrm{g\,cm^{-2}}$)
01	76.2	189	2.13
02	86.8	183	2.59
03	86.6	188	2.45
04	70.3	183	2.10
05	75.8	192	2.06
06	103.6	193	2.78
07	100.3	196	2.61
08	89.0	176	2.87
09	69.9	182	2.11
10	74.4	178	2.35
11	71.1	178	2.24
12	62.9	174	2.08
13	79.0	186	2.28
Mean value	80.45	184.46	2.36
Standard deviation	12.14	6.91	0.28

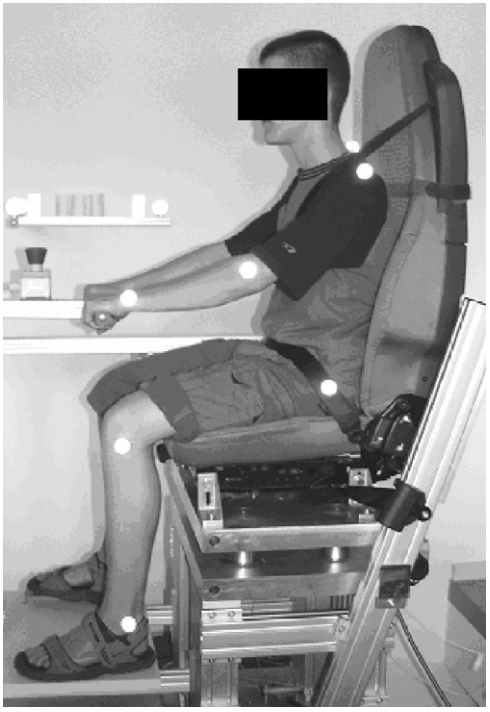

Fig. 1. A male subject sitting in the upper part of the seat, mounted on a Kistler force plate.

on an ENDEVCO 7990 block. The data acquisition (sampling rate 1 ms) was performed by a WaveBook 516 together with WBK16 data acquisition system, both made by IOtech, USA and connected to a standard notebook with IOtech acquisition software. Hardware anti-aliasing filter with a cut-off frequency of 225 Hz preceded the analogue-to-digital conversion. The time series of the measured forces were corrected by subtracting the product of mass of the plate resting on the force sensors (total mass 32.2 kg) and the measured acceleration at the seat plate for all conditions tested.

2.3. Experimental data processing

The apparent mass was calculated by the cross-spectral density method using a Matlab® routine together with the associated coherencies ρ. The mean values of the moduli and phases of the individual apparent masses were calculated by the commonly used averaging method. The curves of the individual apparent mass functions are shown in Fig. 4 for the three vibration intensities tested. The associated coherence functions ρ are depicted in Fig. 2 separately for each intensity. It is seen that the coherence is larger then 0.90 in the frequency band between 0.5 and 30 Hz, indicating sufficient vibratory signal input and good signal-to-noise ratio. Note the dip in Fig. 2a at approximately 27 Hz, which corresponds to subject no. 13. This indicates that the value of the apparent mass function for subject 13 at about 27 Hz is not associated with the excitation acceleration; possible caused by involuntary movement.

The apparent mass functions were calculated from the experimentally measured time responses of acceleration and force. However, throughout the following text the shortened term ''measured apparent mass'' will be used instead. The ''measured'' apparent mass functions will be later on compared to simulated/identified apparent mass functions.

In addition to above measurements, a single test subject (no. 11) was measured on a rigid platform and on the test seat while exposed to random excitation *e*3. Differences in the transfer functions were observed (c.f. Fig. 3). Note the shift in magnitude of the apparent mass peak around 2 Hz due to the cushioned seat upper part, approximately by the value of seat mass. Note also a second peak at 22 Hz when the subject sat on the cushioned seat upper part. This indicates a possible structural resonance in the seat upper part. It should

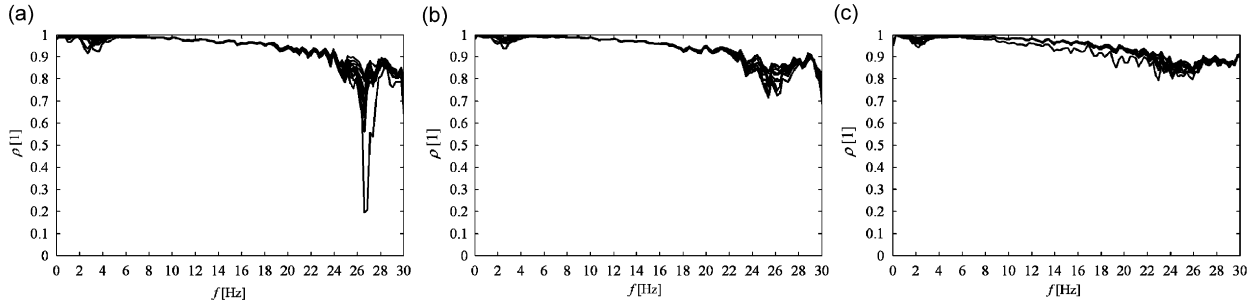

Fig. 2. Coherence function ρ for three excitation intensities used: (a) $e1 = 0.30\,\mathrm{m\,s^{-2}}$; (b) $e2 = 0.98\,\mathrm{m\,s^{-2}}$; (c) $e3 = 1.92\,\mathrm{m\,s^{-2}}$.

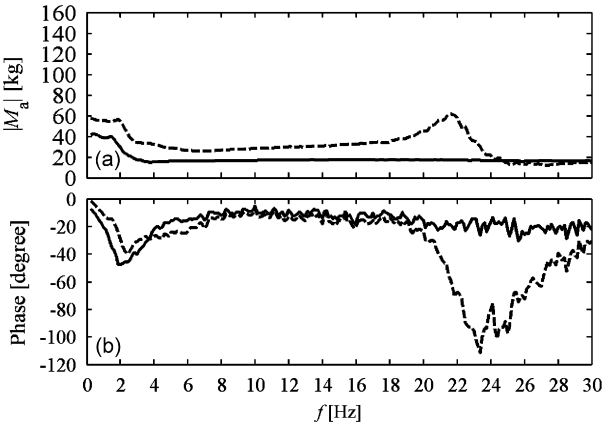

Fig. 3. Comparison of apparent masses in the y-direction for subject no. 11 sitting on the rigid force plate (——) and in the cushioned seat mounted on the force plate (— —) for intensity $e3 = 1.92\,\mathrm{m\,s^{-2}}$: (a) modulus; (b) phase.

not be associated with the human body sitting in the seat. A detailed investigation into the possible causes of this peak was not pursued in this study.

The measured apparent masses of the 13 subjects for the three intensities $e1$, $e2$, $e3$ used are depicted in Fig. 4. As with previous studies [22,30], the frequency band of interest was limited to 0.25–10 Hz. Note the outlier courses (either in the modulus or phase), which for each intensity were obtained for a different subject—subject no. 13 for intensity $e1$, subject no. 7 for intensity $e2$, and subject no. 9 for intensity $e3$. The results for these subjects were discarded, giving a dataset of 12 subjects for each of the three intensities for further analysis.

The mean value, the maxima, minima, and standard deviations (SDs) of the magnitudes and phases of the apparent masses of the 12 subjects were calculated in the frequency range between 0.25 and 10 Hz (Fig. 5). The inter subject variability due to height, mass, sitting position, body tonus, etc. of the 12 subjects is generally averaged out.

The averaged apparent mass courses have two adjacent peaks in the low frequency region. One peak occurs approximately at 0.75 Hz, the other one at some 2.75 Hz. These peaks are clearly visible for lower intensities $e1$ and $e2$, but the low frequency peak seems not to be present for the high intensity $e3$. A shift toward lower frequency with increased excitation intensity is visible. There is a slight indication of a further peak around 5.0 Hz.

3. Parameters identification method used

The parameters identification follows the same general approach as described in [30]. The y-direction apparent mass data were made available as N data points in the frequency domain between 0.25 and 10 Hz

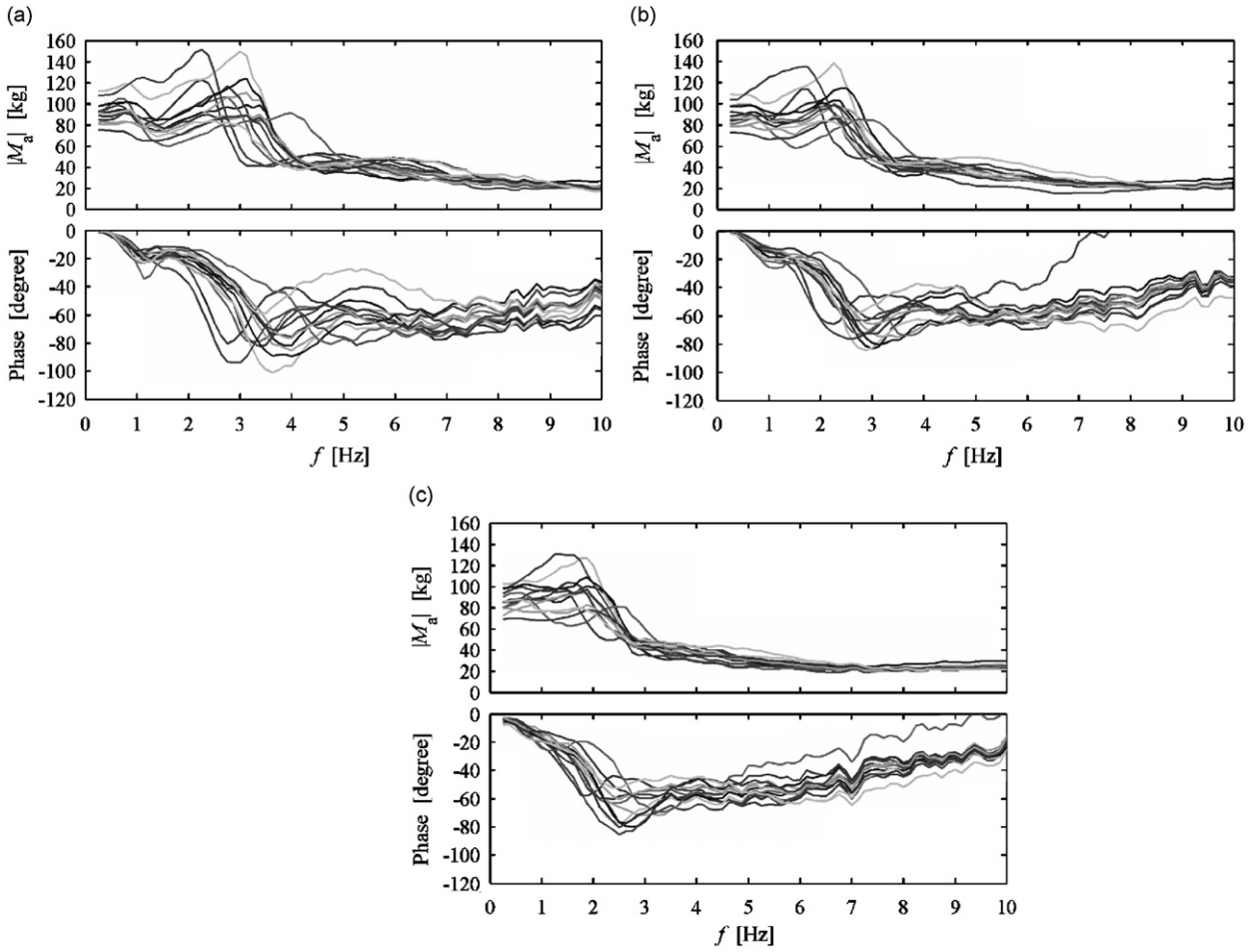

Fig. 4. Measured apparent masses magnitude and phase: (a) $e1 = 0.30\,\mathrm{m\,s^{-2}}$; (b) $e2 = 0.98\,\mathrm{m\,s^{-2}}$; (c) $e3 = 1.92\,\mathrm{m\,s^{-2}}$.

(frequency increment 0.125 Hz). At each frequency f_i the difference d_i between the simulated $\mathbf{M}_{\mathrm{asim}_i}$ and measured apparent mass $\mathbf{M}_{\mathrm{ameas}_i}$ in the complex plane was calculated. The standard least squares method was used to minimise the objective function QE, being the sum of squares of distances d_i. Then

$$\mathrm{QE} = \frac{1}{N}\sum_{i=1}^{N} d_i^2 = \frac{1}{N}\sum_{i=1}^{N}(\mathrm{Re}\{\mathbf{M}_{\mathrm{asim}_i}\} - \mathrm{Re}\{\mathbf{M}_{\mathrm{ameas}_i}\})^2 + (\mathrm{Im}\{\mathbf{M}_{\mathrm{asim}_i}\} - \mathrm{Im}\{\mathbf{M}_{\mathrm{ameas}_i}\})^2 \Rightarrow \min. \tag{3}$$

The standard error ε_a ($\varepsilon_a = \sqrt{\mathrm{QE}}$) of the simulated apparent mass $\mathbf{M}_{\mathrm{asim}}(\omega)$ allows assessment of goodness of fit in the same mass units as the measured variable $\mathbf{M}_{\mathrm{ameas}}(\omega)$. A relative error measure $\mathrm{RE}_{\mathrm{avg}}$ was introduced too, defined as:

$$\mathrm{RE}_{\mathrm{avg}} = \frac{1}{N}\sum_{i=1}^{N}\left|\frac{\mathbf{M}_{\mathrm{ameas}_i} - \mathbf{M}_{\mathrm{asim}_i}}{\mathbf{M}_{\mathrm{asim}_i}}\right| \times 100 \quad [\%]. \tag{4}$$

The MATLAB® function *fminsearch* from the Optimisation Toolbox® was used, based on Nelder and Mead simplex algorithm [34]. The function was modified to facilitate constrained optimisation, i.e. limiting the search to a parameters subspace representing physically meaningful values (positive masses and stiffnesses). The complex numerical value of $\mathbf{M}_{\mathrm{asim}}(\omega_i)$ for each frequency f_i ($\omega_i = 2\pi f_i$) was calculated using formulas for

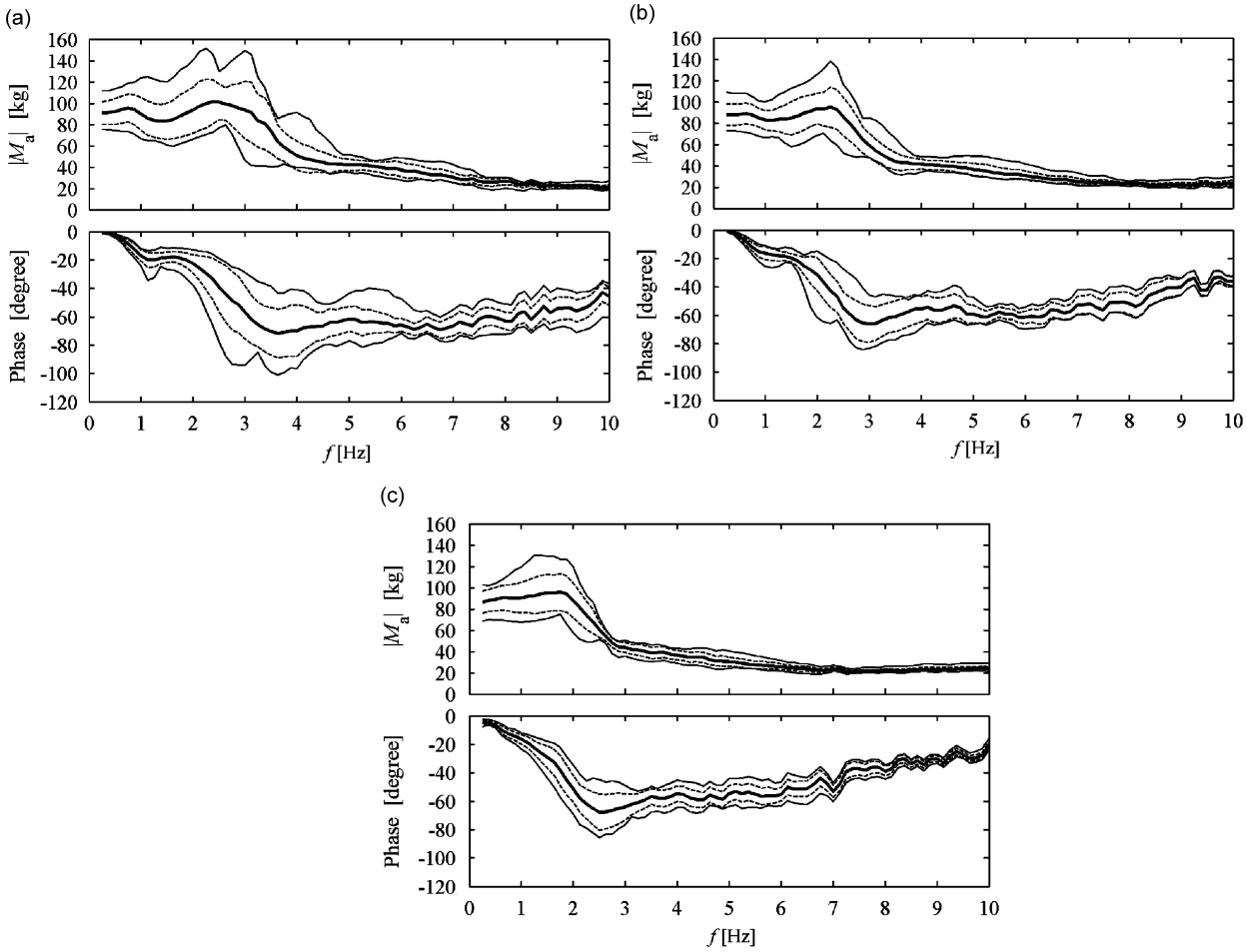

Fig. 5. Measured apparent mass: mean (——); min and max (—); mean ± SD (– –); (a) $e1 = 0.30\,\mathrm{m\,s^{-2}}$; (b) $e2 = 0.98\,\mathrm{m\,s^{-2}}$; (c) $e3 = 1.92\,\mathrm{m\,s^{-2}}$.

the apparent mass $\mathbf{M}_a$, to be derived from the equations describing the respective mechano-mathematical model of human body sitting in the cushioned seat upper part.

In fact, two approaches were used for analysis of the measured data, as deemed appropriate:

(i) Parameter identification of each subject's apparent mass using selected model and averaging the parameters and error variables to arrive at the *across the subjects apparent mass*. This approach allows the assessment of the inter-subject variability influence on the particular parameters values.
(ii) Calculating the mean apparent mass out of the individual subject apparent masses, identifying the parameters of the *mean apparent mass* for the selected model and calculating the mean error variables. By this averaging process the inter subject variability is averaged out.

4. Model analysis and parameters identification

4.1. Model analysis using a series 3-dof models

In analogy to the previous study by Stein et al. [30], it was hypothesised that it is not possible to consider the combined human body sitting in cushioned seat upper part as separate seat and human body subsystems. Further, it was hypothesised that the interaction with the steering wheel and pedals, which is predominantly in

the fore-and-aft direction, would have minimal influence onto human dynamic behaviour in the lateral direction. Hence:

- The seat frame, in which the seat cushion and seat-back cushion are integrated, was assumed sufficiently rigid in the frequency band to be analysed.
- The human body was considered as a lumped parameter linear model without going into detailed description of various human body segments.
- The interaction with pedals was neglected at this stage; however the interaction with the steering wheel was included, if found further relevant.

Based on these considerations, a 3-dof series model of the seat cushion–human torso system in the y-direction was proposed. The model consists of translatory mechano-mathematical elements only and includes a possible link to the steering wheel. The model structure is depicted in Fig. 6.

The variables are:

m_f	equivalent mass, corresponding to the seat upper part
m_1, k_1, c_1	equivalent mass, equivalent stiffness and equivalent damping coefficients corresponding to the human body in contact with the seat back
m_2, k_2, c_2	equivalent mass, equivalent stiffness and equivalent damping coefficients corresponding to the human body torso not in contact with the seat-back (e.g., upper torso/chest)
m_3, k_3, c_3	equivalent mass, equivalent stiffness and equivalent damping coefficients corresponding to the human body part not in contact with the back support situated in some vertical distance from the seat-back (e.g., head)
k_4, c_4	equivalent stiffness and damping coefficient accounting for the reaction of the human body to the steering wheel
y_b	displacement of the simulator platform in the y-direction
y_1, y_2, y_3	assumed displacements of different parts of the human body

The driver's feet and part of the legs were not supported by the seat but were supposed moving in the same manner in the y-direction, as did the mock-up steering wheel. Hence, the sum $(m_f+m_1+m_2+m_3)$ should be smaller than the mass of the respective test subject m_t plus mass of the seat upper part m_s.

The equations of motion of the model shown in Fig. 6 were formulated as follows:

$$m_1\ddot{y}_1 + k_1(y_1 - y_b) + c_1(\dot{y}_1 - \dot{y}_b) + k_2(y_1 - y_2) + c_2(\dot{y}_1 - \dot{y}_2) = 0, \tag{5a}$$

$$m_2\ddot{y}_2 + k_2(y_2 - y_1) + c_2(\dot{y}_2 - \dot{y}_1) + k_4 y_2 + c_4\dot{y}_2 + k_3(y_2 - y_3) + c_3(\dot{y}_2 - \dot{y}_3) = 0, \tag{5b}$$

$$m_3\ddot{y}_3 + k_3(y_3 - y_2) + c_3(\dot{y}_3 - \dot{y}_2) = 0, \tag{5c}$$

where $\ddot{y}_i$, $\dot{y}_i$, y_i are in turn the y-direction time dependent acceleration, velocity and displacement of the respective i-th model mass m_i.

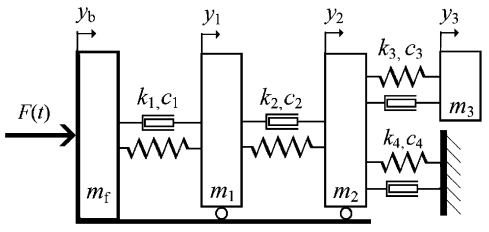

Fig. 6. Simplified translational human body model in a cushioned upper part of a driver's seat, accounting for the bond to the steering wheel—model A.

The resultant time dependent force F at the seat frame in the y-direction is derived from the equation of motion for mass m_f:

$$F = m_f\ddot{y}_b + k_1(y_b - y_1) + c_1(\dot{y}_b - \dot{y}_1). \tag{6}$$

The solution of Eqs. (5) and (6) yields

$$F = m_f\ddot{y}_b + m_1\ddot{y}_1 + m_2\ddot{y}_2 + m_3\ddot{y}_3 + k_4y_2 + c_4\dot{y}_2. \tag{7}$$

Assuming zero initial conditions, Fourier transforms of equations of motion (5) have the form:

$$[m_1(\mathrm{j}\omega)^2 + (c_1 + c_2)(\mathrm{j}\omega) + (k_1 + k_2)]\mathbf{Y}_1(\mathrm{j}\omega) - [c_2(\mathrm{j}\omega) + k_2]\mathbf{Y}_2(\mathrm{j}\omega) - [c_1(\mathrm{j}\omega) + k_1]\mathbf{Y}_b(\mathrm{j}\omega) = 0, \tag{8a}$$

$$[m_2(\mathrm{j}\omega)^2 + (c_2 + c_3 + c_4)(\mathrm{j}\omega) + (k_2 + k_3 + k_4)]\mathbf{Y}_2(\mathrm{j}\omega) - [c_2(\mathrm{j}\omega) + k_2]\mathbf{Y}_1(\mathrm{j}\omega) - [c_3(\mathrm{j}\omega) + k_3]\mathbf{Y}_3(\mathrm{j}\omega) = 0, \tag{8b}$$

$$[m_3(\mathrm{j}\omega)^2 + c_3(\mathrm{j}\omega) + k_3]\mathbf{Y}_3(\mathrm{j}\omega) - [c_3(\mathrm{j}\omega) + k_3]\mathbf{Y}_2(\mathrm{j}\omega) = 0. \tag{8c}$$

The respective complex transfer functions $\mathbf{H}_{1b}(\mathrm{j}\omega) = \mathbf{Y}_1(\mathrm{j}\omega)/\mathbf{Y}_b(\mathrm{j}\omega)$, $\mathbf{H}_{2b}(\mathrm{j}\omega) = \mathbf{Y}_2(\mathrm{j}\omega)/\mathbf{Y}_b(\mathrm{j}\omega)$ and $\mathbf{H}_{3b}(\mathrm{j}\omega) = \mathbf{Y}_3(\mathrm{j}\omega)/\mathbf{Y}_b(\mathrm{j}\omega)$ are derived from Eqs. (8a)–(8c), respectively. Then, the complex apparent mass $\mathbf{M}_a(\omega)$ of multi-body oscillatory system after Fig. 6 is the ratio of the force evaluated according to Eq. (7) (in complex form) to the acting acceleration in the y-direction, i.e., to $\ddot{y}_b$:

$$\begin{aligned}\mathbf{M}_a(\omega) &= \frac{\mathbf{F}(\omega)}{\mathbf{a}(\omega)} \\ &= \frac{m_f\mathbf{Y}_b(\mathrm{j}\omega)^2 + m_1\mathbf{Y}_1(\mathrm{j}\omega)^2 + m_2\mathbf{Y}_2(\mathrm{j}\omega)^2 + c_4\mathbf{Y}_2(\mathrm{j}\omega) + k_4\mathbf{Y}_2 + m_3\mathbf{Y}_3(\mathrm{j}\omega)^2}{\mathbf{Y}_b(\mathrm{j}\omega)^2} \\ &= m_f + m_1\mathbf{H}_{1b}(\mathrm{j}\omega) + m_2\left[1 - \frac{k_4}{\omega^2 m_2} - \mathrm{j}\frac{c_4}{\omega m_2}\right]\mathbf{H}_{2b}(\mathrm{j}\omega) + m_3\mathbf{H}_{3b}(\mathrm{j}\omega).\end{aligned} \tag{9}$$

This is the formula for the Fig. 6 model apparent mass for comparison with the measured data.

The proposed 3-dof structure according to Fig. 6, referred to as model A, was simplified to examine the possibility of reducing the degrees of freedom without seriously impairing accuracy and still retaining a plausible biodynamic model. The proposed link to the mock-up steering wheel, described by parameters k_4, c_4, was considered. However, in paper [30] it was shown for the x-direction that the values of respective elements k_x and c_x have a large spread around a mean value, the coefficient of variation of k_x and c_x being at least of the order of 130 and 40 percent, respectively. This was attributed to involuntary homeostatic behaviour of the human body. Moreover, if for the fore-and-aft direction a link seems not to be plausible, it is even less plausible that a link essentially acting in the x-axis should have any influence in the cross y-axis. Hence, based on these considerations, the next step was to remove the link described by mechano-mathematical elements k_4 and c_4. This results in a model structure as depicted in Fig. 7, are referred to as model B.

The apparent mass formula (9) was then modified, as the term in square bracket for this case equals to one, to give

$$\mathbf{M}_a(\omega) = m_f + m_1\mathbf{H}_{1b}(\mathrm{j}\omega) + m_2\mathbf{H}_{2b}(\mathrm{j}\omega) + m_3\mathbf{H}_{3b}(\mathrm{j}\omega). \tag{10}$$

It was assumed that mass m_f represents the full mass of the cushioned seat upper part m_s. Hence, m_f was constrained to $m_s = 20.8\,\mathrm{kg}$ and proceed further with so constrained identification.

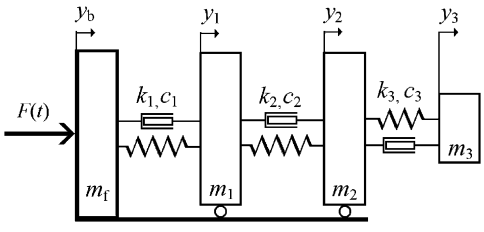

Fig. 7. Simplified translational human body model in a cushioned upper part of a driver's seat—model B.

Table 2
Identification based on apparent mass mean values for models A and B.

Intensity	m_f (kg)	m_1 (kg)	m_2 (kg)	m_3 (kg)	$\sum m_i$ (kg)	k_1 (N m^{-1})	c_1 (N s m^{-1})	k_2 (N m^{-1})	c_2 (N s m^{-1})	k_3 (N m^{-1})	c_3 (N s m^{-1})	k_4 (N m^{-1})	c_4 (N s m^{-1})	ε_a (kg)	RE$_{avg}$ (%)
Model A															
$e1$	13.9	34.8	22.8	13.4	84.9	34930	740.8	10692	298.2	440.6	64.6	0	3.8	2.62	5.7
$e2$	20.4	20.1	28.8	11.5	80.8	29089	289.7	7857	355.7	295.4	49.5	0	3.8	3.56	11.1
$e3$	20.0	19.8	33.9	7.5	81.2	22482	350.6	5784	369.7	176.9	30.8	0	15.4	3.16	9.8
Model B															
$e1$	12.9	48.3	10.9	13.1	85.2	25090	865.4	6925	58.4	417.9	63.7	–	–	2.17	4.5
$e2$	15.9	40.8	12.4	12.8	81.9	17977	662.8	5117	70.2	269.8	60.2	–	–	2.23	6.2
$e3$	17.5	40.9	12.0	14.6	85.0	12168	543.9	4205	61.0	156.7	76.8	–	–	2.59	8.1
Model B ($m_f = 20.8$ kg)															
$e1$	20.8	23.7	27.9	14.7	87.1	39309	290.7	11750	394.2	457.4	74.3	–	–	3.55	9.1
$e2$	20.8	28.2	20.1	14.4	83.5	23329	391.3	6849	190.8	291.9	72.7	–	–	3.18	9.7
$e3$	20.8	29.2	19.1	18.0	87.1	16313	376.8	5620	163.5	141.1	104.0	–	–	3.06	9.8

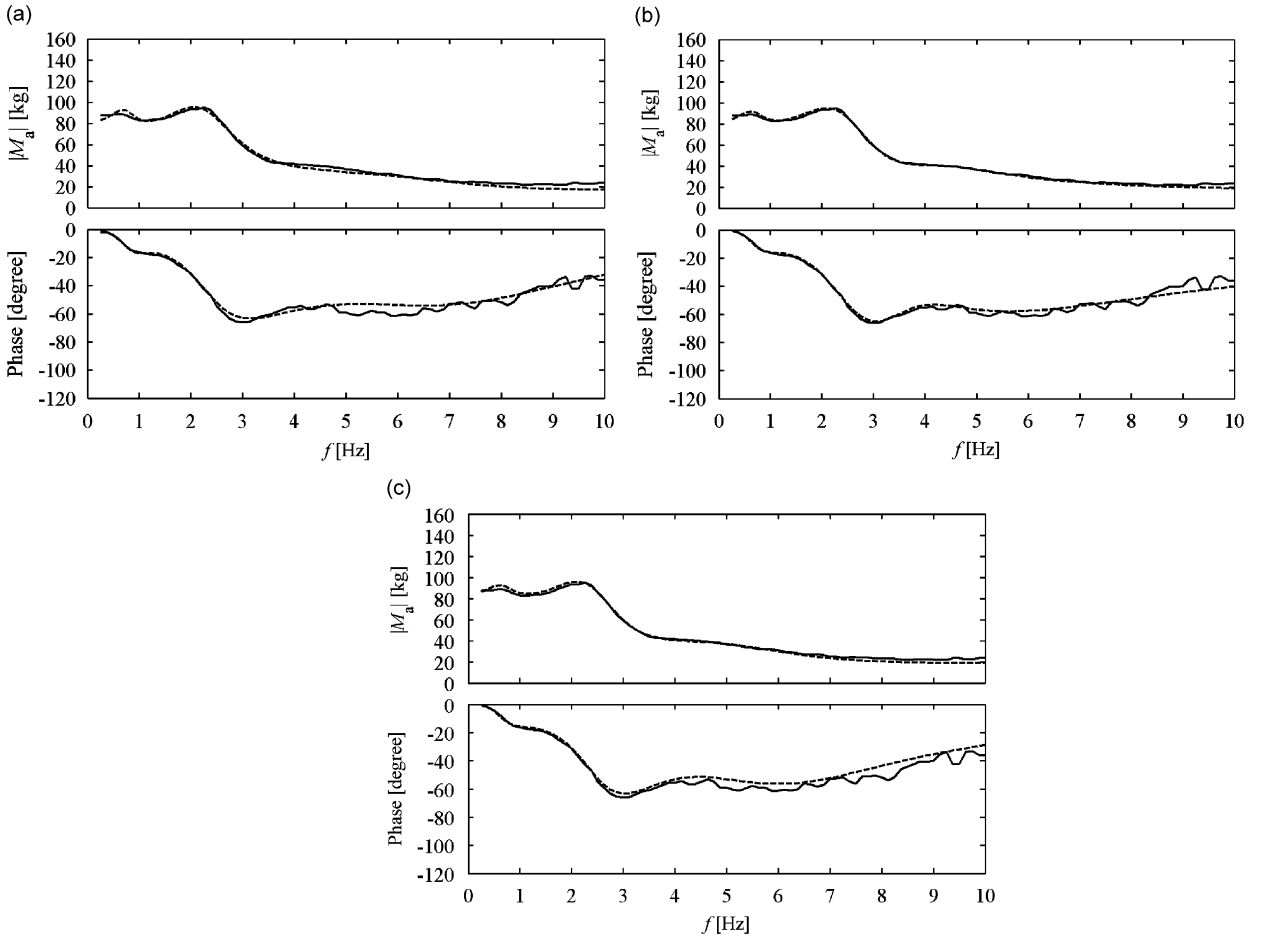

Fig. 8. Courses of simulated (– –) and mean measured (—) apparent mass modulus and phase for excitation intensity $e2 = 0.98$ m s^{-2}; (a) model A; (b) model B; (c) model B with fixed m_f.

The results of the parameter optimisation of models A and B were carried out according to the procedure described in Section 3 and are presented in Table 2 and in Fig. 8. Simulated and averaged apparent masses are shown in turn for each model. Inspecting respective error variables in last columns of Table 2 it can be seen that model B performs best; some minute differences at higher frequencies in Figs. 8a–c also indicate better match for the model B. Fixing of the frame mass m_f worsens the error variables values. Based on the last two columns of Table 2, it was inferred that the model B outperforms model A. The link described by parameters k_4 and c_4 should be excluded and no predetermined mass m_f should be used. Hence, the result of this step is the preference for model B after Fig. 7.

4.2. Model analysis using other types of 3-dof models

As suggested from this measurement and literature sources [4,14,17], 3-dofs models are required to adequately describe the measured apparent mass courses. To explore all possibilities in finding the 'best' model, other structures must also be analysed. The best model would give the smallest error variables ε_a, $\mathrm{RE}_{\mathrm{avg}}$ values.

The following model structures were examined further:

(i) A serio-parallel mechano-mathematical structure, depicted in Fig. 9, denoted model C.
(ii) A fully parallel structure, depicted in Fig. 10, denoted model D.

The respective variables introduced in Fig. 10 could have following meaning:

m_f	equivalent mass, corresponding to the mass of seat upper part
m_1, k_1, c_1	equivalent mass, equivalent stiffness and equivalent damping coefficients corresponding to the human body torso in contact with the seat-back (e.g., back and upper torso)
m_2, k_2, c_2	equivalent mass, equivalent stiffness and equivalent damping coefficients corresponding to the human body part not in contact with the seat-back situated in some vertical distance from the seat back (e.g., head/chest)
m_3, k_3, c_3	equivalent mass, equivalent stiffness and equivalent damping coefficients corresponding to the lower part human body in contact with the seat-back (e.g., pelvis and upper thighs)
y_b	displacement of the simulator platform in the y-direction
y_1, y_2, y_3	assumed displacements of different parts of the human body.

The model D of Fig. 10 has no resemblance to distinguishable human body segments and is a fully mechano-mathematical structure enabling to use the modal approach, as described in some depth in [12].

The formulas for complex apparent mass $\mathbf{M}_a(\omega)$ may be derived in analogical way as described above.

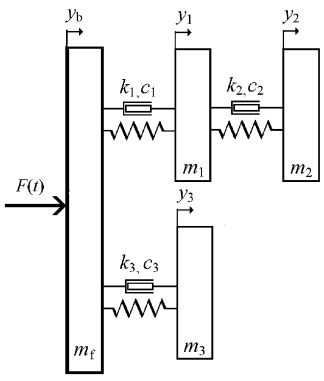

Fig. 9. A serio-parellel apparent mass model—model C.

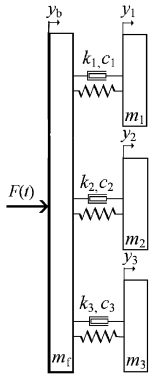

Fig. 10. A fully parallel apparent mass model—model D.

For the serio-parallel model C of Fig. 9 the equations of motions are:

$$m_1\ddot{y}_1 + k_1(y_1 - y_b) + c_1(\dot{y}_1 - \dot{y}_b) + k_2(y_1 - y_2) + c_2(\dot{y}_1 - \dot{y}_2) = 0, \tag{11a}$$

$$m_2\ddot{y}_2 + k_2(y_2 - y_1) + c_2(\dot{y}_2 - \dot{y}_1) = 0, \tag{11b}$$

$$m_3\ddot{y}_3 + k_3(y_3 - y_b) + c_3(\dot{y}_3 - \dot{y}_b) = 0. \tag{11c}$$

For the fully parallel model D of Fig. 10 the equations of motions are as follows:

$$m_1\ddot{y}_1 + k_1(y_1 - y_b) + c_1(\dot{y}_1 - \dot{y}_b) = 0, \tag{12a}$$

$$m_2\ddot{y}_2 + k_2(y_2 - y_b) + c_2(\dot{y}_2 - \dot{y}_b) = 0, \tag{12b}$$

$$m_3\ddot{y}_3 + k_3(y_3 - y_b) + c_3(\dot{y}_3 - \dot{y}_b) = 0. \tag{12c}$$

The resultant time dependent force F at the seat frame in the y-direction was computed from the equation of motion for mass m_f:

$$F = m_f\ddot{y}_b + m_1\ddot{y}_1 + m_2\ddot{y}_2 + m_3\ddot{y}_3. \tag{13}$$

Respective complex transfer functions $\mathbf{H}_{1b}(\mathrm{j}\omega) = \mathbf{Y}_1(\mathrm{j}\omega)/\mathbf{Y}_b(\mathrm{j}\omega)$, $\mathbf{H}_{2b}(\mathrm{j}\omega) = \mathbf{Y}_2(\mathrm{j}\omega)/\mathbf{Y}_b(\mathrm{j}\omega)$ and $\mathbf{H}_{3b}(\mathrm{j}\omega) = \mathbf{Y}_3(\mathrm{j}\omega)/\mathbf{Y}_b(\mathrm{j}\omega)$ were derived from equations of motions (11) and (12) in the same way as above and then used for calculation of respective apparent mass $\mathbf{M}_a(\omega)$:

$$\mathbf{M}_a(\omega) = \frac{\mathbf{F}(\omega)}{\mathbf{a}(\omega)} = \frac{m_f\mathbf{Y}_b(\mathrm{j}\omega)^2 + m_1\mathbf{Y}_1(\mathrm{j}\omega)^2 + m_2\mathbf{Y}_2(\mathrm{j}\omega)^2 + m_3\mathbf{Y}_3(\mathrm{j}\omega)^2}{\mathbf{Y}_b(\mathrm{j}\omega)^2}, \tag{14a}$$

$$\mathbf{M}_a(\omega) = m_f + m_1\mathbf{H}_{1b}(\mathrm{j}\omega) + m_2\mathbf{H}_{2b}(\mathrm{j}\omega) + m_3\mathbf{H}_{3b}(\mathrm{j}\omega). \tag{14b}$$

The identification procedure was the same as above.

5. Selection of the best model

Having found the optimal parameters (Table 3) for each of the models either way, it was possible to compare the respective optimal apparent mass courses (magnitudes and phases), using either Eqs. (10) or (14b). The frequency of expressed maxima in the measured apparent masses modulus for each model was

examined. This was done graphically as shown in Fig. 11 for excitation intensity $e2$ and the mean values of respective identified parameters. Fig. 11 consists of the following:

(i) Upper row: respective transfer functions modules $\mathbf{H}_{1b}$, $\mathbf{H}_{2b}$, $\mathbf{H}_{3b}$ for each model.
(ii) Lower row: graphical comparison (modulus and phase) of the measured courses (solid) and the simulated ones (dashed).

For clarity the error variables ε_a, $\mathrm{RE}_{\mathrm{avg}}$ for models B, C, and D are summarised in Table 4 for both the mean apparent mass and for the across the subjects mean apparent mass.

From the identified and measured apparent mass in the lower part of the Fig. 11 a marked difference in model C performance can be seen: the discrepancies between the measured and simulated mean apparent mass courses (both magnitude and phase) are marked, especially at the lower frequencies. The error variables for both approaches obtained for model C are mostly larger then those obtained for models B and D. Hence, based on these observations, the model C was discarded. From Table 4 it can also be seen that the error variables for the across subject approach are generally slightly larger than the error variables for the mean apparent mass courses.

From Table 4 it can be concluded that there were no marked preference for any of the two models B or D, based on error variables values. There were no visible discrepancies between simulated and measured apparent mass courses (see Fig. 11). However, the following should be noted:

- Model B is based on the idea of finding a model, resembling the human torso, and enabling an approximate association of respective oscillatory modes with human body segments. Due to its series structure, this model naturally includes interactions between the respective oscillatory modes. These interactions are clearly seen from the courses of the respective transfer functions in the upper part of Fig. 11a.
- Model D is a pure mathematical model, without any resemblance of human body segments. It allows the de-coupling of the respective oscillatory modes of the analysed system, hence the model does not account for any interactions. This is clearly seen in the upper part of from Fig. 11c. It is similar in form to the 'preferred' model from [27].

Model B is more justified than model D from the biodynamic point of view. Hence, based on the paper basic aim, the mechano-mathematical model B, resembling a little the human body torso, is preferred to a pure mechano-mathematical model D.

Table 3
Identification based on apparent mass mean values for models B–D.

Intensity	m_f (kg)	m_1 (kg)	m_2 (kg)	m_3 (kg)	$\sum m_i$ (kg)	k_1 ($\mathrm{N\,m^{-1}}$)	c_1 ($\mathrm{N\,s\,m^{-1}}$)	k_2 ($\mathrm{N\,m^{-1}}$)	c_2 ($\mathrm{N\,s\,m^{-1}}$)	k_3 ($\mathrm{N\,m^{-1}}$)	c_3 ($\mathrm{N\,s\,m^{-1}}$)	ε_a (kg)	$\mathrm{RE}_{\mathrm{avg}}$ (%)
Model B													
$e1$	12.9	48.3	10.9	13.1	85.2	25090	865.4	6925	58.4	417.9	63.7	2.17	4.5
$e2$	15.9	40.8	12.4	12.8	81.9	17977	662.8	5117	70.2	269.8	60.2	2.23	6.2
$e3$	17.5	40.9	12.0	14.6	85.0	12168	543.9	4205	61.0	156.7	76.8	2.59	8.1
Model C													
$e1$	13.9	60	10.7	5.3	89.9	17378	866.9	377.6	36.5	26.9	0.0	5.03	10.6
$e2$	15.7	56.2	9.4	3.6	84.9	10828	723.8	215.0	29.5	61.5	24.0	4.92	11.4
$e3$	17.6	39.5	27.3	0.2	84.6	10241	580.2	149.4	368.1	19.5	22.8	4.39	11.3
Model D													
$e1$	14.2	39.9	7.4	24.7	86.2	12653	432.9	10517	180.8	842.2	153.6	2.56	5.5
$e2$	15.8	24.9	7.5	35.0	83.6	5691	185.9	7154	162.7	856.8	330.2	2.24	6.2
$e3$	17.5	30.8	3.5	32.8	84.6	4564	233.5	2811	52.3	712.3	272.7	2.66	8.2

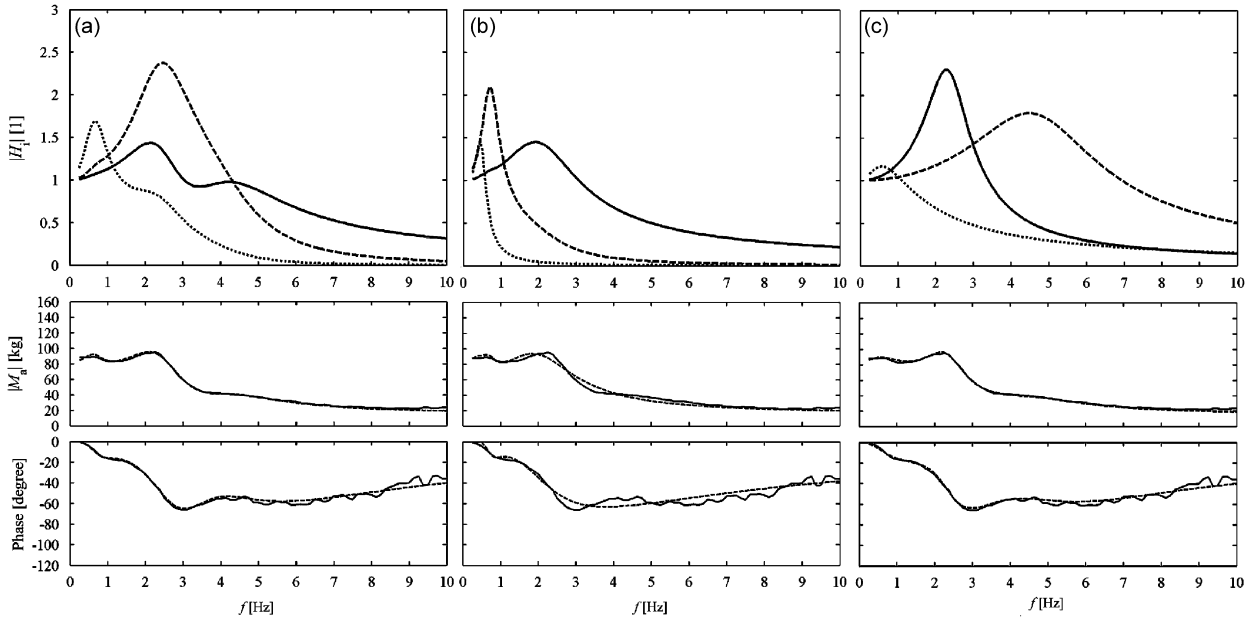

Fig. 11. Courses of transfer functions: $\mathbf{H}_{1b} = \mathbf{Y}_1/\mathbf{Y}_b$ (——), $\mathbf{H}_{2b} = \mathbf{Y}_2/\mathbf{Y}_b$ (— —), $\mathbf{H}_{3b} = \mathbf{Y}_3/\mathbf{Y}_b$ (…) and the simulated (– –) and mean measured (—) apparent mass modulus and phase for excitation intensity $e2 = 0.98\,\mathrm{m\,s^{-2}}$: (a) model B; (b) model C; (c) model D.

Table 4
Estimated errors for models B–D.

Method	Intensity	ε_a (kg)			$\mathrm{RE}_{\mathrm{avg}}$ (%)		
		Model B	Model C	Model D	Model B	Model C	Model D
Across	$e1$	3.75	8.73	4.04	8.5	15.4	9.1
	$e2$	3.28	7.00	2.81	8.7	13.9	7.6
	$e3$	3.23	5.22	3.12	9.7	13.1	9.5
Mean	$e1$	2.17	5.03	2.56	4.5	10.6	5.5
	$e2$	2.23	4.92	2.24	6.2	11.4	6.2
	$e3$	2.59	4.39	2.66	8.1	11.3	8.2

For sake of completeness the parameter values obtained for intensities $e1$, $e2$, $e3$ using the chosen model B of Fig. 7 are presented in Tables 5–8. At the end of each table the mean value (Mean), the standard deviation (SD) and the coefficient of variation (VAR (percent)) are given.

6. Discussion

6.1. Analysis of literature sources on y-axis apparent mass measurements

The measured apparent mass data used in this study were based on measurement with realistic commercially available cushioned seat upper part with back contact in the lumbar region only, described in more detail in [33]. Hence, the apparent mass measurement results using rigid seats are not fully compatible with those of single axis y-direction excitation as reported in [4,17,19,20,22]. However, some comparison is still possible. In [4] results two peaks appear, one beyond 1.0 Hz and another one around 2.5 Hz. The second peak is also

Table 5
Identified model parameters for excitation $e1 = 0.30\,\mathrm{m\,s^{-2}}$ (rms).

Subject	Mass (kg)	Height (cm)	m_f (kg)	m_1 (kg)	m_2 (kg)	m_3 (kg)	$\sum m_i$ (kg)	k_1 ($\mathrm{N\,m^{-1}}$)	c_1 ($\mathrm{N\,s\,m^{-1}}$)	k_2 ($\mathrm{N\,m^{-1}}$)	c_2 ($\mathrm{N\,s\,m^{-1}}$)	k_3 ($\mathrm{N\,m^{-1}}$)	c_3 ($\mathrm{N\,s\,m^{-1}}$)	ε_a (kg)	$\mathrm{RE_{avg}}$ (%)
1	76.2	189	13.0	43.7	11.2	16.2	84.1	32865	771.7	7774	8.7	471.7	80.9	3.6	7.6
2	86.8	183	15.2	42.9	13.9	16.3	88.3	25521	659.4	6626	40.4	467.0	63.9	3.13	7.7
3	86.6	188	14.0	42.0	18.7	11.4	86.1	27536	736.0	5497	68.8	283.9	35.2	2.45	6.2
4	70.3	183	13.0	37.3	15.1	10.7	76.1	32462	688.2	9886	99.3	371.1	48.7	2.63	5.8
5	75.8	192	11.2	44.7	15.2	10	81.1	32043	866.1	7241	60.2	381.2	47.4	3.03	5.4
6	103.6	193	18.7	36.6	28.3	21.3	104.9	39359	483.0	17675	221.8	697.1	123.3	6.82	13.2
7	100.3	196	16.2	52.1	20.9	10.3	99.5	22750	585.4	7291	62.8	543.7	52.8	3.47	9.5
8	89.0	176	18.1	24.0	30.4	17.4	89.9	41051	512.7	18336	343.9	642.9	87.4	4.81	11.2
9	69.9	182	16.0	36.8	7.6	17.6	78.0	32238	581.5	9539	73.7	715.2	72.7	4.73	10.2
10	74.4	178	14.6	43.5	8.8	12.7	79.6	24038	734.4	6819	26.7	521.3	71.2	3.8	8.4
11	71.1	178	15.5	41.5	6.8	10.4	74.2	24516	623.9	5031	1.7	517.9	54.2	3.81	9.8
12	62.9	174	13.2	32.3	13.1	12.1	70.7	38474	626.4	7445	65.0	236.4	60.1	2.77	6.7
Mean	80.6	184.3	14.9	39.8	15.8	13.9	84.4	31071	655.7	9096.7	89.4	487.5	66.5	3.75	8.5
SD	12.7	7.2	2.2	7.1	7.6	3.7	10.1	6292.3	110.4	4387.3	98.1	152.3	23.3	1.22	2.4
VAR	15.7	3.9	14.7	17.8	47.9	26.9	12.0	20.3	16.8	48.2	109.7	31.2	35.1	32.55	28

Subject no. 13 excluded.

Table 6
Identified model parameters for excitation $e2 = 0.98\,\mathrm{m\,s^{-2}}$ (rms).

Subject	Mass (kg)	Height (cm)	m_f (kg)	m_1 (kg)	m_2 (kg)	m_3 (kg)	$\sum m_i$ (kg)	k_1 ($\mathrm{N\,m^{-1}}$)	c_1 ($\mathrm{N\,s\,m^{-1}}$)	k_2 ($\mathrm{N\,m^{-1}}$)	c_2 ($\mathrm{N\,s\,m^{-1}}$)	k_3 ($\mathrm{N\,m^{-1}}$)	c_3 ($\mathrm{N\,s\,m^{-1}}$)	ε_a (kg)	$\mathrm{RE_{avg}}$ (%)
1	76.2	189	16.1	36.9	15.9	13.3	82.2	19577	604.6	6351	52.1	353.0	59.0	2.81	7.9
2	86.8	183	16.7	40.4	14.5	16.6	88.2	17621	559.9	5041	51.5	357.1	68.1	3.14	8.6
3	86.6	188	14.6	41.5	15.5	6.3	77.9	18355	663.5	3318	62.8	74.8	49.2	5.38	12
4	70.3	183	16.0	32.7	16.5	9.0	74.2	20147	527.3	7609	154.6	362.1	50.3	2.64	7.6
5	75.8	192	13.9	40.7	16.7	9.3	80.6	20299	718.5	4751	108.9	233.5	49.9	2.18	6.1
6	103.6	193	18.5	48.1	18.0	15.1	99.7	20487	619.2	6940	91.8	285.7	60.7	4.48	10.7
8	89.0	176	21.3	35.2	18.4	14.6	89.5	19716	475.0	8966	168.9	385.9	64.8	4.66	12.7
9	69.9	182	15.9	20.1	22.3	15.7	74.0	33425	545.0	12457	311.3	502.5	56.5	3.38	8.6
10	74.4	178	17.9	37	12.9	10.2	78.0	15998	544.6	5243	76.5	264.4	42.9	3.12	8.9
11	71.1	178	16.9	37.6	8.7	9.1	72.3	16037	543.5	3725	37.3	220.9	39.1	3.03	8.2
12	62.9	174	15.8	29.3	13.3	10.3	68.7	23780	508.8	4888	76.6	157.7	46.7	2.34	7.2
13	79.0	186	13.4	35	16.3	15.3	80.0	29544	709.7	4753	78.4	290.8	71.0	2.25	5.9
Mean	78.8	183.5	16.4	36.2	15.8	12.1	80.4	21249	585.0	6170.2	105.9	290.7	54.9	3.28	8.7
SD	11.0	6.2	2.1	7.0	3.3	3.4	8.6	5288	78.6	2557.6	76.1	113	10.1	1.03	2.1
VAR	14.0	3.4	13.0	19.2	21.2	28.2	10.7	24.9	13.4	41.5	71.8	38.9	18.4	31.35	24.5

Subject no. 7 excluded.

reported in [27]; however, not the first one, which was probably caused because the frequency band of interest was above 1.5 Hz, i.e., not covering the first peak at all. Both authors discussed the appearance of a further peak around 5 Hz; however, this peak seems to be excitation amplitude dependent and not present in some measurements. The results presented by [17] for the no-back and the vertical back support, pertinent to the seat pan, indicate two peaks for the lower intensity vibration $0.25\,\mathrm{m\,s^{-2}}$ rms (at 0.77 and 2.05 Hz) and $0.5\,\mathrm{m\,s^{-2}}$ rms (at 0.94 and 2.1 Hz), too, but not for the high intensity excitation of $1.0\,\mathrm{m\,s^{-2}}$. The distinction between these two peaks is more apparent for the no-back condition.

Table 7
Identified model parameters for excitation $e3 = 1.92\,\mathrm{m\,s^{-2}}$ (rms).

Subject	Mass (kg)	Height (cm)	m_f (kg)	m_1 (kg)	m_2 (kg)	m_3 (kg)	$\sum m_i$ (kg)	k_1 ($\mathrm{N\,m^{-1}}$)	c_1 ($\mathrm{N\,s\,m^{-1}}$)	k_2 ($\mathrm{N\,m^{-1}}$)	c_2 ($\mathrm{N\,s\,m^{-1}}$)	k_3 ($\mathrm{N\,m^{-1}}$)	c_3 ($\mathrm{N\,s\,m^{-1}}$)	ε_a (kg)	$\mathrm{RE_{avg}}$ (%)
1	76.2	189	18.8	30.4	18.6	15.2	83	16886	400.1	5986	93.8	247.8	72.0	3.21	10.3
2	86.8	183	17.9	40.4	12.9	14.3	85.5	11766	498.8	3256	50.6	209.1	56.8	2.83	8.8
3	86.6	188	18.1	36.4	21.2	13.1	88.8	13836	485.4	2796	105.6	181.6	55.8	3.41	11.1
4	70.3	183	17	38.4	9.0	12.2	76.6	10351	481.5	5465	66.6	18.7	84.0	2.71	8.7
5	75.8	192	15.6	41.4	15.0	10.6	82.6	13091	583.9	3159	97.2	39.8	46.7	2.75	8.5
6	103.6	193	18.6	47.9	18.0	14.6	99.1	15140	589.4	5032	94.1	159.8	59.7	4.02	11.2
7	100.3	196	18.2	50.6	12.8	19.7	101.3	11936	457.1	5728	35.4	93.0	140	3.64	11.2
8	89.0	176	22.2	42.4	12.7	14.5	91.8	12755	441.7	4760	49.8	294.9	68.4	4.65	12.6
10	74.4	178	18.1	24.3	26.4	10.6	79.4	14009	465.2	7315	253.8	382.3	57.7	3.6	10.8
11	71.1	178	17.9	33.8	10.1	11.5	73.3	12421	473.4	3234	47.5	163.9	53.3	2.82	8.6
12	62.9	174	16.3	28.3	12.3	14.2	71.1	15679	527.4	4479	92.8	49.3	58.1	2.50	7.6
13	79.0	186	15.6	31.9	15.7	19.3	82.5	20693	571.0	4039	99.8	183.7	86.3	2.59	7.4
Mean	81.3	184.7	17.9	37.2	15.4	14.2	84.6	14047	497.9	4604.2	90.6	168.7	69.9	3.23	9.7
SD	12.2	7.2	1.8	7.9	5.0	3.0	9.4	2774.6	59.1	1377.0	57.0	108.3	25.2	0.66	1.7
VAR	15.1	3.9	9.8	21.2	32.2	20.9	11.1	19.8	11.9	29.9	62.9	64.2	36.0	20.36	17.1

Subject no. 9 excluded.

Table 8
Identified model B parameters of mean and for across the subjects apparent masses.

Method	Intensity	Mass (kg)	Height (cm)	m_f (kg)	m_1 (kg)	m_2 (kg)	m_3 (kg)	$\sum m_i$ (kg)	k_1 ($\mathrm{N\,m^{-1}}$)	c_1 ($\mathrm{N\,s\,m^{-1}}$)	k_2 ($\mathrm{N\,m^{-1}}$)	c_2 ($\mathrm{N\,s\,m^{-1}}$)	k_3 ($\mathrm{N\,m^{-1}}$)	c_3 ($\mathrm{N\,s\,m^{-1}}$)	α (%)
Mean	$e1$	80.6	184.3	12.9	48.3	10.9	13.1	85.2	25090	865.4	6925	58.4	417.9	63.7	84
	$e2$	78.8	183.5	15.9	40.8	12.4	12.8	81.9	17977	662.8	5117	70.2	269.8	60.2	82
	$e3$	81.3	184.7	17.5	40.9	12.0	14.6	85.0	12168	543.9	4205	61.0	156.7	76.8	83
Across	$e1$	80.6	184.3	14.9	39.8	15.8	13.9	84.4	31071	655.7	9098	89.4	487.5	66.5	83
	$e2$	78.8	183.5	16.4	36.2	15.8	12.1	80.4	21249	585.0	6170	105.9	290.7	54.9	81
	$e3$	81.3	184.7	17.9	37.2	15.4	14.2	84.6	14047	497.9	4604	90.6	168.7	69.9	83

Mansfield and Maeda [20] published a thorough study on single axis and multi axis random acceleration excitation with two rms values 0.4 and $0.8\,\mathrm{m\,s^{-2}}$ for the back-off and the back-on condition (a rigid upright standing back support). Fifteen subjects took part in this study. The median resonance frequency for the back-on condition was 2.0 and 1.5 Hz for excitation intensity 0.4 and $0.8\,\mathrm{m\,s^{-2}}$, respectively, whereas the same peaks were observed at 1.75 and 1.5 Hz for the back-off condition. Due to limitations of the experimental equipment, the low frequency peak around 0.75 Hz could not be measured. There is a discrepancy with the results presented in [17], obtained under similar conditions, however with different excitation intensities. It could be speculated that the main cause is the nonlinear behaviour of the human body, presentation of different characteristics (mean value versus median value) and, maybe, different physical characteristics of the test subjects, too.

6.2. Analysis of y-axis apparent mass mean value courses

Following observations can be made from the experimentally determined mean apparent mass moduli courses, used in this study, which are highlighted once more in Fig. 12, obtained with the resolution in frequency 0.125 Hz:

(i) For intensity $e1$ two peaks are present—one at 0.75 Hz, the other one at 2.50 Hz.
(ii) For intensity $e2$ two peaks are present—one at 0.63 Hz, the other one at 2.25 Hz.

(iii) For intensity $e3$ the peak at lover frequency is hardly observable at 0.63 Hz, whereas the other peak is clearly seen at 1.75 Hz.
(iv) The dominant peak between 1.75 and 2.50 Hz shifts toward lower frequencies as the excitation intensity increases. The peak height decreases with increased intensity.
(v) The peak around 0.70 Hz shifts toward lower frequency with increase of excitation. Peak height changes are rather marginal.
(vi) An inexpressive peak around 5–6 Hz for the lower intensities $e1$ and $e2$ could be seen; however, this peak virtually diminishes for the high intensity $e3$.

These results are similar to the findings of Mandapuram et al. [17]. There is qualitative agreement of the present study with the findings of Fairley and Griffin [4] and, with the above-mentioned reservation, to the study [27]. There are some differences to the study [20] as for similar intensities and the back-on condition they have found the dominant peak at a frequency some 0.4 and 0.7 Hz lower, respectively, than in this study. The cause is not fully understood but possible reasons are given above. The measurements also underline strong dependence of the third peak position and occurrence on excitation intensity. It can be concluded that the measurements used for this study are in agreement with those of the previous studies, quoted.

In Table 9 the natural damped frequencies are presented. Note the shift in respective frequencies in respect to excitation intensity, as observed experimentally. It should be noted that the discrepancies between the damped natural frequencies and the position of measured peaks in the apparent mass courses are understandable because of the series structure of the model. The masses m_3, m_2 in turn influence the dynamic behaviour of the oscillatory system described by k_1, c_1, as clearly seen in the upper part of Fig. 11a. This would not be the case for the modally de-coupled model D, as seen in the upper part of Fig. 11c. Hence, the analysis of model eigenfrequencies, especially for model B, is of minor importance and is only of informative nature.

In Ref. [22] apparent mass measurements with the same group of subjects, subjected to three random excitations (nearly flat spectrum from 0.25 to 30 Hz for 65 s) with mean unweighted rms values $e1 = 0.29\,\mathrm{m\,s^{-2}}$, $e2 = 0.99\,\mathrm{m\,s^{-2}}$, and $e3 = 1.85\,\mathrm{m\,s^{-2}}$ were reported. The same apparatus was used; however, the subjects were sitting directly on the Kistler force plate, i.e. without the cushioned seat upper part. This gives the opportunity to compare the courses of the measured apparent mass with the cushioned seat (Fig. 12) and without the cushioned seat (Fig. 3b in Ref. [22]). The respective maxima position on the frequency axis can be assessed:

(i) For the intensity $e1$ two maxima are clearly seen, one at approximately 0.54 Hz; the second one at 2.04 Hz. A very inexpressive peak can be assumed at approximately 4.5 Hz.
(ii) For the intensity $e2$ there is a peak at approximately 0.71 Hz and another one at 1.74 Hz; however, the third one is not present.

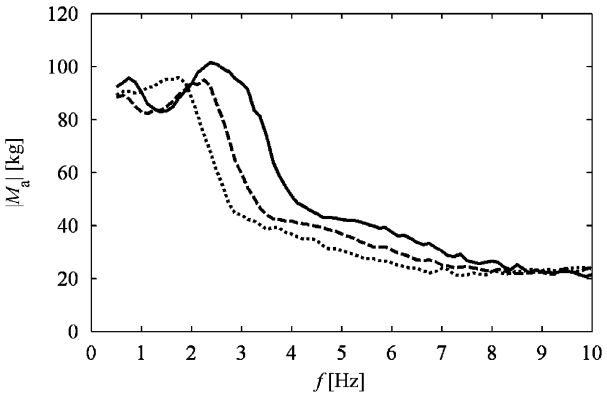

Fig. 12. Comparison of the measured mean apparent masses for the three intensities tested: $e1 = 0.30\,\mathrm{m\,s^{-2}}$ (——); $e2 = 0.98\,\mathrm{m\,s^{-2}}$ (— —); $e3 = 1.92\,\mathrm{m\,s^{-2}}$ (…).

Table 9
Natural damped frequencies for model B based on the mean apparent mass parameters.

Intensity	Natural damped frequencies		
	f_{1d} (Hz)	f_{2d} (Hz)	f_{3d} (Hz)
$e1$	4.7	2.9	0.8
$e2$	4.0	2.4	0.6
$e3$	3.5	1.9	0.3

(iii) For the intensity $e3$ an inexplicit maximum between 0.62 and 1.40 Hz is seen.
(iv) The inexpressive peak at 4.5 Hz is not present for higher intensities. The reason for that could be an increasing body tension with the increase in excitation intensity [22].

It can be concluded that the frequencies, corresponding to the first peak are more-or-less the same (with large spread); whereas the second peak frequencies are slightly higher in this study, then those determined for subjects sitting on a rigid seat and follow the same, intensity dependent, tendency.

6.3. Comparison of modelled y-direction apparent mass with previous models

As already mentioned, the only study, dealing with y-direction apparent mass modelling, is that one by Mansfield and Lundström [27]. Their study is based on apparent mass measurements with no back support under different conditions as used in the present study; hence, a direct comparison of the obtained value is not possible. Essentially the same model structure as models B–D used here were presented in their study, augmented by the same type of models with mass $m_f = 0$ kg. It was argued that the parallel structure, similar to model D (Fig. 10), albeit with mass $m_f = 0$ kg, best described the measured data. As only the apparent mass modulus data were used for identification larger errors might have been introduced than those observed in the present study. Moreover, a poor phase match above around 4 Hz was seen in respective figures in [27]. Here both the modulus and phases match is reasonable throughout the analysed frequency band 0.25–10 Hz, which is much wider than that one used in the study [27].

In addition to the identification the three proposed models reported in this study, variants with $m_f = 0$ kg were also tested. The match between the simulated and measured apparent mass course was inferior to those with $m_f \neq 0$ kg. In addition, the error variables ε_a and $\mathrm{RE}_{\mathrm{avg}}$ were much larger, i.e., worse. This outcome is understandable—in the study [27] no cushioned seat with a back support was used, hence essentially no mass m_f was required; whereas in this study a rather massive seat upper part of mass $m_s = 20.8$ kg was present. The seat upper part mass should in some way be included in the apparent mass formula. This observation also supports the approach followed in here.

6.4. Model parameters dependence on excitation intensity

Table 8 was compiled to summarise the simulation results with the model B. Table 8 allows the assessment of the intensity dependence of the identified parameters. For the mean parameters, there is no intensity dependent pattern observable in the mass distribution among the particular masses m_1, m_2, m_3 changes. Their sum remains approximately constant, as is the total sum $\sum m_i$. Note the influence of removal of subject no. 7 (mass $m_t = 100.3$ kg), exhibiting erroneous input data, from the analysed group of persons in comparison to exclusion of lighter subject (nos. 13 or 9, respectively) on the value of $\sum m_i$.

There was a small, intensity dependent, change in the mass of the frame. The value of parameter m_f is less than the weight of seat upper part $m_s = 20.8$ kg. The sum of masses m_f, m_1, m_2, m_3 is smaller than the averaged test subject mass m_t plus the mass of the seat upper part m_s. This indicates that the soft seat cushion and the cushioned seat-back comprise only a certain part of the sum of test subject mass m_t and seat upper part mass m_s. It can be hypothesised that the seat itself does not support feet and partly legs and hence the total mass subjected to horizontal inertial forces is lower than the sum $m_t + m_s$. From the last column of Table 8 follows,

that the proportion α of the sum of model masses to the sum m_t+m_s, calculated after Eq. (15), expressed in percent, is of the order of 81–84 percent.

$$\alpha = \frac{m_f + m_1 + m_2 + m_3}{m_s + m_t} \times 100 \quad [\%]. \tag{15}$$

From Fig. 12 and Table 8 some further indicative conclusions on excitation intensity dependence can be drawn. In Fig. 12 a difference in response to the lower intensities $e1$ and $e2$ than to the higher intensity $e3$, is seen: with increased intensity the inexpressive peak around 5 Hz diminishes completely. Note small stiffness and damping constant values for the third dof in comparison to respective values for the other two dofs. This dof caters for the very low frequency component.

There was an intensity dependent change in stiffnesses k_1, k_2 and in damping coefficient c_1 observable. The multi-body oscillatory system essentially "softens" in respect to increased excitation intensity. No intensity dependent pattern in damping constants c_2, c_3 is observable.

7. Conclusions

From the analysed apparent mass measurements in the y-direction with a group of 13 male test subjects exposed to three excitation intensities following conclusions can be drawn:

The measured apparent mass data can be modelled using standard linear translatory mechano-mathematical "building blocks"—positive masses m_i, positive stiffnesses k_i, and linear viscous damping coefficients c_i. It was shown that the best model representation is that one of a three-degree-of-freedom linear oscillatory system with intensity dependent parameters, partially accounting for the nonlinear dynamic properties of the human body. The response of the model chosen (see Fig. 7) is in line with previous observations, indicating the presence of three resonance peaks: first around some 0.7 Hz, the second one around 2.5 Hz, and an inexpressive one at approximately 5.0 Hz. The position of these peaks on the frequency axis is shifted a little towards higher frequencies in comparison to corresponding peaks in apparent mass functions obtained under similar conditions but without the cushioned seat upper part.

The model accounts for human body sitting in the upright position on a cushioned seat upper part with a cushioned seat-back support. It accounts for the stipulated human body segments. There are only few, if any, measurements with a group of test subjects in this practically important test person position. Except for the study by Mansfield and Lundström [27], there are few, if any, other studies dealing with y-direction human body apparent mass modelling. It is believed, that this is the first study with a group of test subjects dealing with modelling of the y-direction apparent mass of human subjects sitting upright in the driver's seat upper part, which is the position driver is supposed to assume in many practical situations.

The parameter identification was performed using both the modulus and phase information in the frequency range 0.25–10 Hz. The phase information was used extensively for parameters identification. This is an advantage of this study, as the inclusion of phase information in the identification studies is often omitted.

The averaged data allowed the calculation of the ratio α of the sum of inertial masses subject to movement in the y-direction to the total mass of the test subject plus the seat upper part, taking into account those parts of the human body (feet and partially legs), which are not exposed to the excitation. The ratio α was established as being approximately 83 percent and so larger than a similar value used for vertical direction studies.

Acknowledgements

The research was conducted within two Partners of the VIBSEAT project, funded by the European Commission FP 5 Growth Programme, coordinated by the Human Factors Research Unit, ISVR, University of Southampton, UK (Contract G3RD-CT-2002-00827) in the period 2002–2005; project coordinator *Professor Michael J. Griffin*. This paper was prepared within works on the Project 2/6161/26 of the VEGA Agency of the Slovak Republic. The support of the European Commission and the Slovak VEGA Agency is acknowledged.

References

[1] D.V. Balandin, N.N. Bolotnik, W.D. Pilkey, *Optimal Protection from Impact, Shock and Vibration*, Gordon and Breach Science Publishers, Amsterdam, 2001.

[2] M.J. Griffin, *Handbook of Human Vibration*, Academic Press, London, 1990.

[3] N.J. Mansfield, *Human Response to Vibration*, CRC Press, Boca Raton, 2005.

[4] T.E. Fairley, M.J. Griffin, The apparent mass of the seated human body in the fore-and-aft and lateral directions, *Journal of Sound and Vibration* 139 (1990) 299–306.

[5] M.J. Griffin (Ed.), Special issue on WBV Injury Conference, *Journal of Sound and Vibration* 215 (4) (1998) 593–996.

[6] M.J. Griffin (Ed.), Special issue on WBV Injury Conference, *Journal of Sound and Vibration* 253 (1) (2002) 1–327.

[7] P.-É. Boileau, S. Rakheja, X. Wu, A body mass dependent mechanical impedance model for applications in vibration seat testing, *Journal of Sound and Vibration* 253 (1) (2002) 243–264.

[8] G. Meltzer, R. Melzig-Thiel, M. Schatte, Ein ebenes mathematisches Schwingungs-modell des sitzenden Mensch, *Maschinenbautechnik* 35 (1986) 513–516.

[9] T.E. Fairley, Predicting the transmissibility of a suspension seat, *Ergonomics* 33 (1990) 121–135.

[10] L. Wei, M.J. Griffin, Mathematical models for the apparent mass of the seated human body exposed to vertical vibration, *Journal of Sound and Vibration* 212 (5) (1998) 855–875.

[11] N. Nawayaseh, Modelling the vertical and fore-and-aft forces caused by whole-body vertical vibration, *Proceedings of the 37th United Kingdom Conference on Human Responses to Vibration*, Leicestershire, UK, 2002, pp. 302–320.

[12] H. Rützel, B. Hinz, H.P. Wölfel, Modal description—a better way of characterising human vibration behaviour, *Journal of Sound and Vibration* 293 (3) (2006) 810–823.

[13] P. Holmlund, R. Lundström, Mechanical impedance of the human body in the horizontal direction, *Journal of Sound and Vibration* 215 (4) (1998) 801–812.

[14] N.J. Mansfield, R. Lundström, The apparent mass of the human body exposed to non-orthogonal horizontal vibration, *Journal of Biomechanics* 32 (1999) 1269–1278.

[15] G. Fleury, Experimentelle Untersuchung der dynamischer Masse einer sitzender Versuchsperson bei Schwingungen in der X-Richtung zur Bildung eines Modells, Tagung "Humanschwingungen" Darmstadt, *VDI Berichte* 1821 (2004) 301–316.

[16] N. Nawayseh, M.J. Griffin, Non-linear dual-axis biodynamic response to fore-and-aft whole-body vibration, *Journal of Sound and Vibration* 282 (3–5) (2005) 831–862.

[17] S.C. Mandapuram, S. Rakheja, M.A. Shiping, R.G. Demont, P.-É. Boileau, Influence of Back Support Conditions on the Apparent Mass of Seated Occupants under Horizontal Vibration, *Industrial Health* 43 (3) (2005) 421–435.

[18] Y. Matsumoto, K. Ohdo, T. Saito, Dynamic and subjective responses of seated subjects exposed to simultaneous vertical and fore-and-aft whole-body vibration: The effect of phase between the two single-axis components, *Journal of Sound and Vibration* 293 (3) (2006) 773–787.

[19] N.J. Mansfield, S. Maeda, Comparison of the apparent masses and cross-axis apparent masses of seated humans exposed to single and dual-axis whole-body vibration, *Journal of Sound and Vibration* 293 (3) (2006) 841–853.

[20] N.J. Mansfield, S. Maeda, The apparent mass of the seated human exposed to single-axis and multi-axis whole-body vibration, *Journal of Biomechanics* 40 (2007) 2543–2551.

[21] N. Nawayseh, M.J. Griffin, Effect of seat surface angle on forces at the seat surface during whole-body vertical vibration, *Journal of Sound and Vibration* 284 (3–5) (2005) 613–634.

[22] B. Hinz, R. Blüthner, G. Menzel, S. Rützel, H. Seidel, H.P. Wölfel, Apparent mass of seated men—determination with single- and multi-axis excitations at different magnitudes, *Journal of Sound and Vibration* 293 (3) (2006) 788–809.

[23] X. Wu, S. Rakheja, P.-É. Boileau, Dynamic performance of suspension seats under vehicular vibration and shock excitations, *Proceedings of SAE International Conference & Exposition*, Paper No. 1999-01-1304, Detroit, USA, 1999.

[24] S. Rakheja, I. Stiharu, P.-É. Boileau, Seated occupant apparent mass characteristics under automotive postures and vertical vibration, *Journal of Sound and Vibration* 253 (1) (2002) 57–75.

[25] B. Hinz, S. Rützel, J. Keitel, G. Menzel, H. Seidel, The apparent mass under automotive posture as a prerequisite for the modelling of the sitting man—results for males and females (in German), Tagung "Humanschwingungen" Darmstadt, *VDI Berichte* 1821 (2004) 57–86.

[26] S. Rakheja, I. Stiharu, H. Zhang, P.-É. Boileau, Seated occupant interactions with seat backrest and pan, and biodynamic responses under vertical vibration, *Journal of Sound and Vibration* 293 (3) (2006) 651–671.

[27] N.J. Mansfield, R. Lundström, Models of the apparent mass of the seated human body exposed to horizontal whole-body vibration, *Aviation and Space Environmental Medicine* 70 (1999) 1166–1172.

[28] G. Fleury, P. Mistrot, Numerical assessment of fore-and-aft suspension performance to reduce whole body vibration of wheel loader drivers, *Journal of Sound and Vibration* 293 (3) (2006) 672–687.

[29] G.J. Stein, P. Múčka, R. Chmúrny, Preliminary results on an *x*-direction apparent mass model of human body sitting in a cushioned suspended seat, *Journal of Sound and Vibration* 293 (3) (2006) 688–703.

[30] G.J. Stein, P. Múčka, R. Chmúrny, B. Hinz, R. Blüthner, Measurement and modelling of *x*-direction apparent mass of the seated human body–cushioned seat system, *Journal of Biomechanics* 40 (2007) 1493–1503.

[31] International Organization for Standardization ISO 5982, Mechanical vibration and shock—range of idealized values to characterize seated-body biodynamic response under vertical vibration, 2001.

[32] International Organization for Standardization ISO 13090-1, Mechanical vibration and shock—guidance on safety aspects of tests and experiments with people—part 1: exposure to whole-body mechanical vibration and repeated shock, 1998.
[33] B. Hinz, R. Blüthner, H. Seidel, G. Menzel, Apparent mass functions of the combination subject/seat—an experimental study, Research Report WP3, EU-Project VIBSEAT, 2005.
[34] Using Matlab, Version 6, The MathWorks, Inc., Natick, Massachusetts, USA, 2004.